

Variability of Graupel and Snow Observed in Tropical Oceanic Convection by Aircraft during TRMM KWAJEX

ELLEN M. SUKOVICH AND DAVID E. KINGSMILL

*University of Colorado, Cooperative Institute for Research in Environmental Sciences, and
NOAA/Earth System Research Laboratory, Boulder, Colorado*

SANDRA E. YUTER

North Carolina State University, Raleigh, North Carolina

(Manuscript received 7 January 2008, in final form 12 August 2008)

ABSTRACT

Empirical characterization of graupel and snow in precipitating tropical convective clouds is important for refining satellite precipitation retrieval algorithms and cloud-resolving and radiative transfer models. Microphysics data for this analysis were collected by the University of North Dakota (UND) Citation and the National Aeronautics and Space Agency (NASA) DC-8 aircraft during the Tropical Rainfall Measuring Mission (TRMM) Kwajalein Experiment (KWAJEX) in the western tropical Pacific Ocean. An ice particle identification algorithm was applied to two-dimensional optical array probe data for the purpose of identifying ice particle ensembles dominated by graupel or snow particles. These ensembles were accumulated along 1-km flight segments at temperatures below 0°C. A third category, mixed graupel/snow, has characteristics between those of the predominately graupel and snow ensembles and can be used either in combination with the other two categories or separately. Snow particle ensembles compose 80% of UND Citation and 98% of NASA DC-8 ensemble data. For the UND Citation, graupel ensembles compose ~5% of the total with mixed graupel/snow ensembles composing ~15%. There were no graupel ensembles in the NASA DC-8 data, which were collected primarily at temperatures < -35°C. Particles too small to classify (<150- μm maximum dimension) compose 56% of UND Citation and 64% of NASA DC-8 particle images. Nearly all these “tiny” particles occur coincident with particles >~150 μm . Combining data from both aircraft, snow and mixed graupel/snow ensembles were evident over the full range of subfreezing temperatures (from 0° to -65°C) sampled by the aircraft. In contrast, graupel ensembles were present primarily at temperatures > -10°C. Accurate graupel identification was further supported by all graupel ensembles observed either coincident with or within a 10-km horizontal distance of radar-identified convective precipitation structures.

1. Introduction

Precipitating convective clouds over the tropical oceans play a major role in the global water and energy balance. Satellite precipitation retrievals are vital for accurate precipitation mapping over the ocean since surface precipitation measurements are sparse. The Tropical Rainfall Measuring Mission (TRMM) (Simpson et al. 1988) is a joint effort of the National Aeronautics and Space Agency (NASA) and the Japanese Space Agency (JAXA) to improve the estimation and characterization of tropical rainfall. Launched in November 1997, the

TRMM satellite (Kummerow et al. 1998, 2000) has a suite of active and passive microwave remote sensors to estimate surface rainfall. Several algorithms have been specifically developed by the TRMM community to derive rainfall products from various sensor combinations. Assumptions regarding the microphysical character of precipitating clouds, particularly the horizontal and vertical distribution of hydrometeor size, shape, phase, and density, are large sources of uncertainty in these algorithms (e.g., Smith et al. 1992; Iguchi et al. 2000; Kummerow et al. 2001). In particular, the physical characteristics of precipitation-size ice in tropical oceanic mixed phase deep convective clouds are poorly understood since there has been little in situ information available. Characterization of ice particles is also critical for validating the cloud-resolving models and

Corresponding author address: David E. Kingsmill, University of Colorado, CIRES, UCB 216, Boulder, CO 80309.
E-mail: david.kingsmill@colorado.edu

radiative transfer models upon which rests the scientific foundation of the TRMM precipitation retrieval algorithms.

Precipitating ice particles are often grouped into two broad categories: graupel and snow (Houze 1993). Graupel is relatively dense, has higher fall speeds, and its presence implies particle growth by accretion of supercooled cloud droplets (e.g., collision-coalescence in the rain layer and riming in the ice layer). Snow particles are much less dense, have lower fall speeds, and their presence implies that vapor diffusion and aggregation are the primary microphysical growth processes. Accretion is associated with convective precipitation regions while vapor deposition and aggregation are associated with stratiform precipitation regions (Houze 1997).

Graupel and snow are two of the ice species typically included in bulk microphysical parameterization (BMP) schemes employed in cloud-resolving and radiative transfer models (e.g., Lin et al. 1983; Rutledge and Hobbs 1983; Reisner et al. 1998; Tao et al. 2003; Thompson et al. 2004). In these schemes, snow is usually defined as a combination of individual and aggregated ice crystals. Accurate prediction of the partition of precipitable ice between graupel and snow is important since more graupel favors faster precipitation fallout (Colle et al. 2005). Several recent studies have focused on using in situ and remote sensing observations to assess the performance of BMP schemes (e.g., Brown and Swann 1997; Colle et al. 2005; Lang et al. 2007; Li et al. 2008). These validation studies found that graupel was overpredicted.

TRMM planned and executed several field campaigns in the tropics and subtropics during 1998 and 1999 with the objective of collecting new observational datasets to validate and improve their precipitation retrieval algorithms (Kummerow et al. 2000). Airborne collection of in situ microphysical datasets was a primary emphasis in these campaigns (Kingsmill et al. 2004), particularly the Kwajalein Experiment (KWAJEX), which took place over the tropical western Pacific Ocean in the vicinity of Kwajalein Atoll from July to September 1999 (Yuter et al. 2005). The KWAJEX in situ microphysics data make up one of the largest ice microphysics datasets for open ocean tropical precipitating clouds obtained to date. This study describes the variability of graupel and snow observed by aircraft during KWAJEX. Section 2 presents an overview of the data and instrumentation employed. Details about the technique used to identify ice particle types are described in section 3. The results of the analysis are presented in section 4. A summary of the study and its primary conclusions are provided in section 5.

2. Data overview

KWAJEX employed three aircraft equipped with suites of microphysical instrumentation: the University of North Dakota (UND) Citation, the National Aeronautics and Space Agency (NASA) DC-8, and the University of Washington (UW) Convair. Aircraft malfunctions grounded the UW Convair for a significant period of time during the project, thus considerably limiting the amount of data that could be collected. As a result, this study does not use data collected by the UW Convair.

The UND Citation flew 26 missions and spent 34.5 h in cloud while the NASA DC-8 flew 28 aircraft missions during KWAJEX spending 35 h in cloud. Safety issues constrained the aircraft from penetrating strong convective cells. To obtain a larger microphysics data sample, flight tracks were preferentially laid out within larger precipitation regions as opposed to isolated convective cells. Hence, the in situ microphysics data are biased toward the stratiform and weaker convective portions of contiguous precipitation regions.

The primary in situ microphysics datasets in this study are imagery obtained from two-dimensional optical array probes (2D-OAP; Knollenberg 1970). Hydrometeor image data collected by the UND Citation were obtained from a Particle Measuring Systems (PMS) two-dimensional cloud probe (2DC) and a Stratton Park Engineering Company (SPEC) High-Volume Precipitation Spectrometer (HVPS). NASA DC-8 2D-OAP instrumentation was composed of two probes produced by Droplet Measurement Technology (DMT): a two-dimensional cloud imaging probe (2D-CIP) and a two-dimensional precipitation imaging probe (2D-PIP). The resolution and size range of particle images completely within the bounds of the optical array are shown in Table 1. Given the coarse resolution of the HVPS data (Lawson et al. 1993) and the fact that the 2D-PIP malfunctioned during a large fraction of the project, our study only uses data from the higher-resolution 2DC and 2D-CIP to identify dominant ice particle types within ensembles of particles. HVPS data were only used to supplement the UND Citation 2DC data at larger particle sizes (i.e., >1.0 mm) for the analysis of maximum particle dimension. All of these data were averaged over approximately 1-km distances along the flight track, which correspond to ~ 10 -s ensembles for the UND Citation and ~ 5 -s ensembles for the NASA DC-8 following the Common Microphysics Product format (Kingsmill et al. 2004).

During KWAJEX, approximately 1.5×10^7 and 6.2×10^7 particle images were collected by the UND Citation 2DC and NASA DC-8 2D-CIP aircraft, respectively.

TABLE 1. Optical array probes used in the TRMM KWAJEX field campaign. Range and resolution (in parentheses) are indicated.

Optical array probe	UND Citation	NASA DC-8
PMS 2DC/DMT 2D-CIP	30–960 μm (30 μm)	25–1600 μm (25 μm)
PMS 2DP/DMT 2D-PIP	N/A	100–6400 μm (100 μm)
SPEC HVPS	200 μm –4.2 cm (200 \times 400 μm)	—

These images were processed with an approach analogous to that employed by Kingsmill et al. (2004), with artifacts such as “streakers” and “gapped images” (e.g., Gordon and Marwitz 1984) eliminated from the image database and partial images sized through a reconstruction technique that assumes circular symmetry (Heymsfield and Parrish 1978). The temperature range of in-cloud sampling by the UND Citation ranged between -45° and 20°C , with 91% of the processed images collected at temperatures less than 0°C (Fig. 1a). NASA DC-8 in-cloud sampling was at higher altitudes and thus lower temperatures, ranging between -65° and 0°C , with 97% of the processed images collected at temperatures less than -35°C (Fig. 1b). To focus the analysis on levels of the cloud where ice particles exist without the complicating effects of melting, the 2DC and 2D-CIP datasets were constrained to temperatures below 0°C .

To place the aircraft in situ microphysics data in the context of the three-dimensional precipitation structure, we use data from the S-band Doppler radar located on Kwajalein Island. Reflectivity (Z) from this radar was mapped onto a Cartesian grid out to a range of 156 km with a horizontal grid spacing of 2 km and a vertical grid extending from 1.5 to 18 km with 1.5-km spacing. Gridded reflectivity data from the 1.5-km level were used as input to an algorithm that objectively classifies precipitating echoes (in this study defined when $Z > 15$ dBZ) as convective or stratiform (Yuter et al. 2005). Analysis of all the convective–stratiform maps over the duration of KWAJEX indicates that precipitating areas were 80% stratiform and 20% convective. Approximately 84% of the UND Citation ensembles and 79% of the NASA DC-8 ensembles were collected within the radar grid and classified with respect to radar precipitation structure. The aircraft-sampled radar pixels were identified by mapping flight tracks onto the nearest pixel in the convective–stratiform maps. Overall, for the UND Citation and NASA DC-8, respectively, 71% and 81% of the ensembles were associated with stratiform precipitation while 29% and 19% were associated with convective precipitation. In sec-

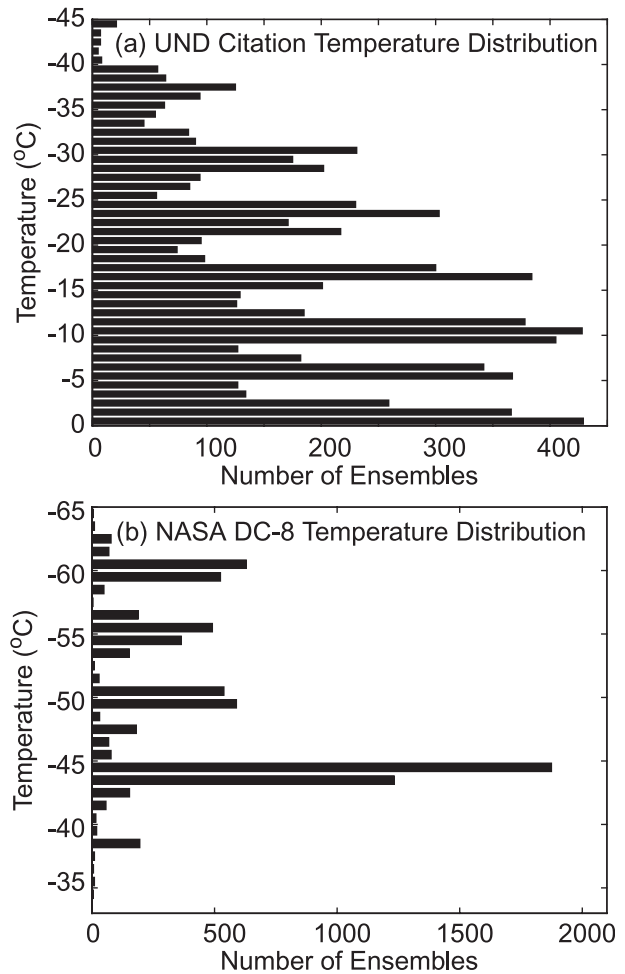


FIG. 1. Ensemble sample size as a function of temperature for particle ensembles containing at least 100 accepted particles for the (a) UND Citation 2DC below 0°C and (b) NASA DC-8 2D-CIP below -35°C during the TRMM KWAJEX field campaign. Local peaks represent air temperatures and altitudes frequently sampled by the aircraft.

tion 4a, we discuss the joint classification of ice particle type and precipitation structure.

3. Ice particle-type identification technique

Several automated algorithms have been developed to objectively identify individual ice particle types for the large number of images that can be collected by 2D-OAPs (e.g., Duroure 1982; Hunter et al. 1984; Holroyd 1987; Moss and Johnson 1994). Inaccuracies and uncertainties in these techniques often limit their utility. One way to work within the framework of these inaccuracies is to take a more statistical approach to the problem by classifying ensembles of particle images rather than individual particle images (e.g., Duroure

TABLE 2. General particle shape categories as defined by Korolev and Sussman (2000).

Category	Description
Sphere	Particles generating circular images, such as liquid drops or quasi-spherical ice particles (e.g., frozen drops, graupel)
Needle	Particles composing elongated quasi-rectangular projections (e.g., columns, needles, rosettes with 3–5 bullets)
Dendrite	Particles including dendrites, stellar crystals, aggregates of dendrites, and spatial dendrites
Irregular	Particles of irregular or random shape that do not fall into any of the above shape categories

et al. 1994). Korolev and Sussman (2000, hereinafter referred to as KS00) employed an ensemble-based scheme for classifying four general particle shapes: “spheres,” “dendrites,” “needles,” and “irregulars” (Table 2), using dimensionless ratios of simple geometric parameters, such as the along- and across-array size of the image and the perimeter and area of the image. Each shape category has an exclusive distribution for each geometric ratio (see KS00 for more detail) and, based on these unique distributions, the KS00 technique derives the fraction of particles within an ensemble having one of their four particle shape categories.

The KS00 technique was applied to KWAJEX 2DC and 2D-CIP particle ensembles that contained images that were completely (“complete”) or largely within (“accepted partial”) the array frame, while images largely outside the array frame (“rejected partial”) and images less than 20 pixels (“tiny”) were excluded from the analysis (Tables 3, 4). The 20-pixel threshold [similar to KS00 and Korolev et al. (2000)] corresponds to quasi-spherical particles with maximum dimensions of $\sim 150 \mu\text{m}$ (UND Citation 2DC, resolution $30 \mu\text{m}$) and $\sim 125 \mu\text{m}$ (NASA DC-8 2D-CIP, resolution $25 \mu\text{m}$). Near and below these size limits, the 2DC and 2D-CIP measurements become less reliable because of depth-of-field uncertainties (Korolev et al. 1998; Strapp et al. 2001). As will be discussed in section 4d, although the tiny images are excluded from the image analysis because they do not contain enough pixels for unambiguous ice particle-type classification (Baumgardner and Korolev 1997), the relative number of these images can be used to help infer microphysical processes that may be active in clouds.

Although the KS00 technique is more statistically robust than previous habit identification algorithms, the generic particle shape categories utilized by KS00 place limitations on the applicability of their algorithm output to particular problems of significance. For example, they do not directly identify graupel within the broader

TABLE 3. Thresholds and limits used by Korolev and Sussman (2000) for data quality control to calculate fractions of sphere, dendrite, needle/column, and irregular particles: N_{total} is the total number of shadowed pixels; N_x is the number of pixels in the x direction; N_y is the number of pixels in the y direction; and N_{edge} is the number of pixels along the edge of the particle image. [See Korolev and Sussman (2000) for further detail.]

KS00 particle classification	Threshold
Tiny particles	$N_{\text{total}} < 20$ pixels
Rejected partial particles	$N_{\text{total}} \leq 180$ pixels $N_{\text{edge}} \geq 4$ pixels $N_y < 32$ pixels
Accepted partial particles	$N_{\text{total}} > 180$ pixels $N_{\text{edge}} \geq 4$ pixels or $N_y = 32$ pixels
Complete particles	$N_{\text{total}} \geq 20$ pixels $N_{\text{edge}} < 4$ pixels

sphere category nor do they identify a snow category similar to those used by bulk microphysical parameterization schemes. In response to this limitation we have developed an algorithm that uses the KS00 output to identify ensembles as one of three ice particle categories: graupel, snow, and mixed graupel/snow.

Figure 2 shows a simple schematic of the ice particle-type discrimination algorithm. Ensembles collected at temperatures below 0°C are required to have a minimum of 100 accepted particles to increase the statistical significance of the results (appendix). Korolev et al. (2000) employed a similar threshold in their particle shape identification analysis. The KS00 sphere fraction (SF) is the key characteristic in distinguishing among graupel ($\text{SF} \geq 0.5$), snow ($\text{SF} < 0.2$), and mixed graupel/snow ($0.2 \leq \text{SF} < 0.5$) particle ensembles, while the KS00 dendrite and needle fractions are used to distinguish between dendrites, needle/columns, and undetermined snow particles within the snow category (Fig. 2). Depending on their application, users can combine the main categories. For example, one can consider the mixed graupel/snow ensembles as part of the graupel

TABLE 4. Calculated percentages and counts (in parentheses) of gap rejected and aspect-ratio rejected (artifacts), tiny, rejected partial, complete, accepted partial, and total number of particle images for the UND Citation 2DC and NASA DC-8 2D-CIP aircraft during the TRMM KWAJEX field campaign.

Particle image type	UND Citation	NASA DC-8
Artifacts	3.4% (508 181)	2.6% (1 598 209)
Tiny	55.7% (8 310 261)	65.4% (40 372 079)
Rejected partial	13.2% (1 970 385)	4.3% (2 639 366)
Complete	24.3% (3 617 788)	27.0% (16 655 810)
Accepted partial	3.4% (503 227)	0.7% (426 660)
Total	100% (14 909 842)	100% (61 692 510)

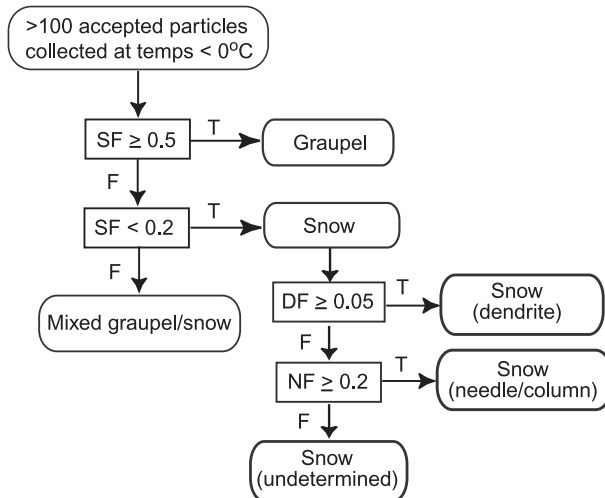


FIG. 2. Ice particle-type identification flowchart for graupel, snow (dendrite, needle/column, undetermined), and mixed graupel/snow particle ensembles utilizing particle-type fraction output obtained from the KS00 habit classification scheme. “SF” is sphere fraction, “DF” is dendrite fraction, and “NF” is needle fraction; “T” indicates condition is true and “F” indicates condition is false.

category, the snow category, or as a separate category. In different combinations the categories can yield error bounds. For the application of validating graupel frequency of occurrence in model output, including the mixed graupel/snow with graupel would yield an overestimate of the presence of graupel, while using the graupel category by itself would yield an underestimate.

Although the KS00 sphere, dendrite, and needle fraction categories are designed to be mutually exclusive, analysis of KWAJEX imagery data indicates that a continuum of ice particle types exists. Figure 3 shows two viewing angles of the three-dimensional scatter of the sphere fraction, dendrite fraction, and needle fraction categories from the UND Citation and the resulting ensemble ice particle-type classifications based on Fig. 2. Rather than distinct clusters of points associated with different ice particle types there is a continuum of characteristics. Hence, the delineation of exact boundaries for automated ice particle-type classification is inherently subjective. The selection of KS00 particle shape fraction thresholds that were used to discriminate among the graupel, snow, and mixed graupel/snow categories was based upon the visual analysis of the dominant ice particle type for a large fraction of the total number of particle ensembles, where ice particle-type dominance is defined as when the occurrence of one ice particle type (graupel or snow) is observed at least twice as much as the other (graupel or snow) within an ensemble. The visual characteristics that were

used to discriminate among the categories are described below.

a. Graupel

The American Meteorological Society’s (AMS) *Glossary of Meteorology* (Glickman 2000) defines graupel as heavily rimed snow particles that are distinguished by conical, hexagonal, and lump forms, which is the definition of graupel used in this analysis. Graupel particles, as viewed by the 2D-OAP, tended to be highly symmetric and largely circular with no appendages or sharp edges.

Ensembles visually determined to be dominated by graupel (Fig. 4a) were found to have sphere fractions greater than or equal to 0.5. The shapes of the individual graupel particles observed in these ensembles are found to range from smooth-edged circular to rougher-edged quasi-circular. There was no graupel observed in the NASA DC-8 sample. UND Citation graupel ensembles had maximum particle dimensions ranging from 150 to $\sim 2000 \mu\text{m}$, due to the reconstruction of images not completely within the optical array domain. For UND Citation ensembles consisting of particles with maximum dimensions between 150 and $\sim 800 \mu\text{m}$, there is sufficient resolution to determine that particles are spherical, but often insufficient resolution to distinguish a smooth versus rough texture of the particle edge, which may indicate supercooled and/or frozen droplets (Czys and Peterson 1992). Because of this limitation of data resolution, the graupel category for this study also includes those particles in the 150–800- μm size range that may be supercooled and/or frozen rain drops.

b. Snow

According to the AMS *Glossary of Meteorology*, snow is “precipitation composed of white or translucent ice crystals, chiefly in complex branch hexagonal form and often agglomerated into snowflakes” (Glickman 2000). Many bulk microphysical schemes use “snow” to refer to any particle that is pristine, irregular, or aggregated (e.g., Lin et al. 1983; Rutledge and Hobbs 1983; Reisner et al. 1998; Tao et al. 2003; Thompson et al. 2004). In this study, the snow category ($\text{SF} < 0.2$) consists of particle ensembles composed of (i) dendrites, stellars, and aggregates of dendrites, (ii) needles, columns, and aggregates of needles and columns, and (iii) other highly irregular and/or randomly shaped particles. We refer to this last group as “undetermined snow particles” to distinguish them from the other two categories, while at the same time noting that our inability to provide a more precise classification of the ice particle type is based on limitations of the observation method (Stoelinga et al. 2007). Particles in the snow category

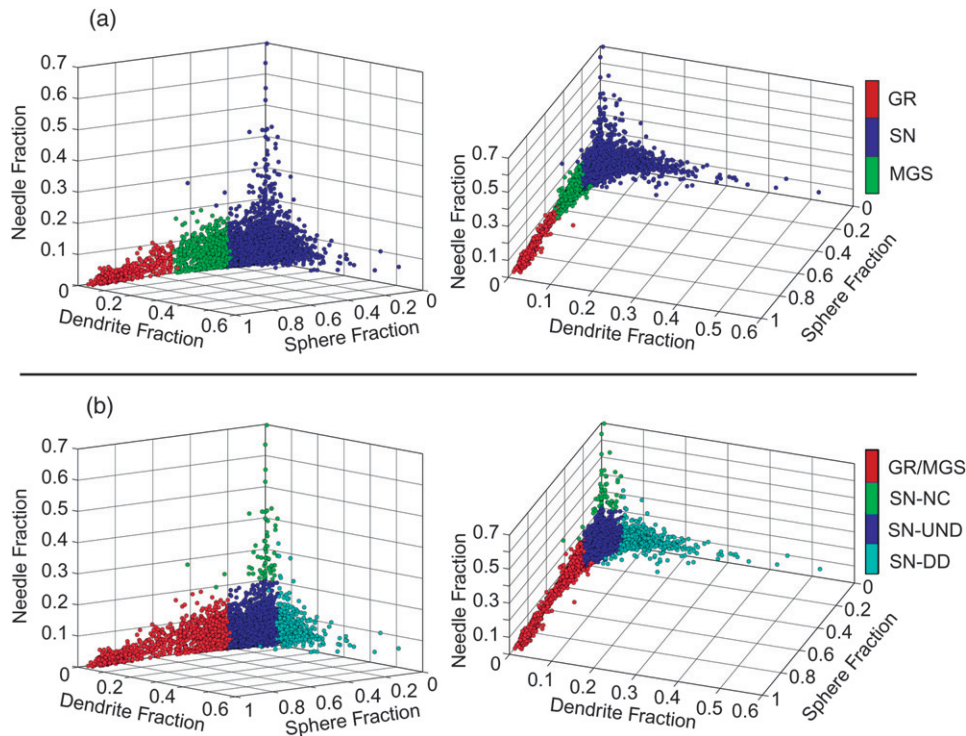


FIG. 3. Two viewing angles of the 3D scatter of the sphere fraction, dendrite fraction, and needle fraction categories and the resulting ensemble habit classifications from the UND Citation based on Fig. 2. (a) Graupel (GR), mixed graupel/snow (MGS), and all snow (SN) particle ensembles. (b) Graupel and mixed graupel/snow combined (GR/MGS), snow-needle/column (SN-NC), snow-undetermined (SN-UND), and snow-dendrite (SN-DD) particle ensembles. The right side of both (a) and (b) is from a higher viewing angle to provide clarity to interpret the plots.

were visually characterized by their appendages, rough edges, irregular shapes, intertwined branches, and porous areas.

Dendrite fraction and needle fraction are used to distinguish among the different types of snow ensembles (Fig. 3b). Those ensembles with a higher dendrite fraction ($DF \geq 0.05$) are classified as snow-dendrite particle ensembles (Fig. 4b), while those with a higher needle fraction ($NF \geq 0.2$) are classified as snow-needle/column particle ensembles (Fig. 4c). The vast majority of the snow ensembles have neither distinct dendrite nor needle characteristics and these particles are classified as snow-undetermined ensembles (Fig. 4e).

Again, depending on the user's application, the subgroups within categories can be combined in various ways. For example, the union of the three snow subgroups yields a large, statistically robust sample size and corresponds to the snow category in bulk microphysics parameterizations where the snow category is composed of individual and aggregated ice crystals of various shapes.

Not surprisingly, ensembles subjectively identified to be dominated by snow-undetermined particles (Fig. 4e) were very well correlated with the KS00 irregular fraction, which in turn was anticorrelated with the KS00 sphere fraction. This anticorrelation between sphere fraction and irregular fraction is strong enough that we do not need to use the irregular fraction as a parameter in our ice particle classification.

c. Mixed graupel/snow

Ensembles classified as mixed graupel/snow (Fig. 3a) contain either a mixture of both graupel and snow particles within the same ensemble or fairly rough-edged and blob-shaped particles that do not fall into either the graupel or snow categories. The mixtures of snow particles and graupel were seldom observed. The more frequently observed ensembles (Fig. 4d) contain particles that lack the appendages, porosity, and larger particle sizes associated with snow particles (Figs. 4b,c,e) but do not have the smooth exteriors and near-circular shapes of graupel (Fig. 4a). These particles often resemble the shape of "graupel-like snow" identified by

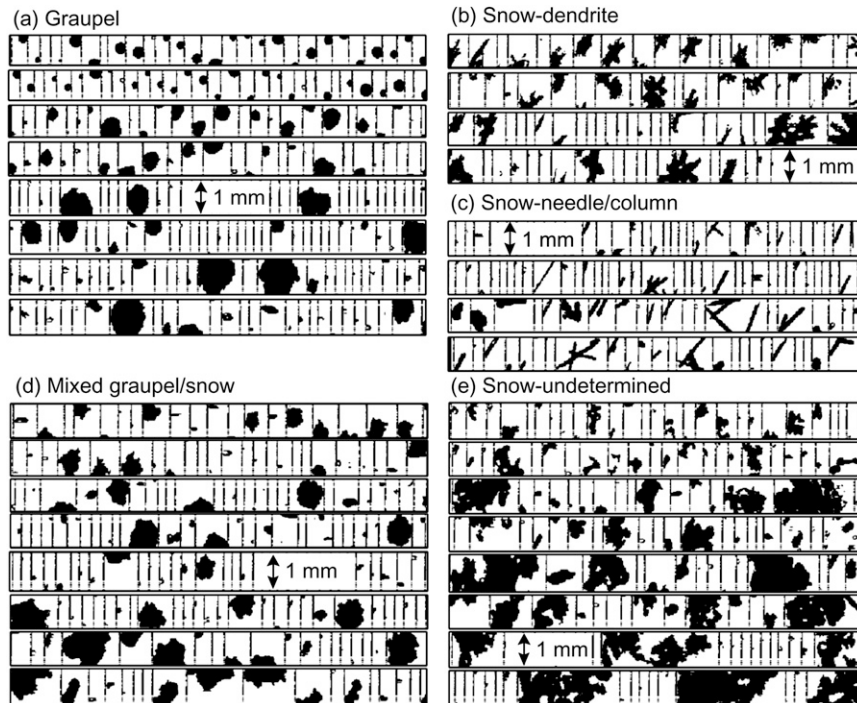


FIG. 4. Selected particle images from the UND Citation 2DC illustrating particle ensembles composed of (a) graupel, (b) snow-dendrite, (c) snow-needle/column, (d) mixed graupel/snow, and (e) snow-undetermined particles.

Locatelli and Hobbs (1974). Particles within these ensembles are hypothesized to be undergoing a transition from snow to graupel.

4. Ice particle-type results

Our analysis of KWAJEX aircraft data used ~ 7600 ensembles ($\sim 4.1 \times 10^6$ particles) of UND Citation 2DC data and ~ 7800 ensembles ($\sim 1.7 \times 10^7$ particles) of NASA DC-8 2D-CIP data accepted for ice particle-type identification. The sample size corresponds well to the 5.6×10^6 images of particles with maximum dimensions greater than $125 \mu\text{m}$ accepted for pattern recognition by Korolev et al. (2000) in their statistical study of ice particle types in stratiform clouds sampled at mid- and high latitudes of North America. Upon application of the ice particle-type discrimination algorithm to these data, the overall KWAJEX UND Citation 2DC ensemble population for particles with maximum dimensions greater than $150 \mu\text{m}$ was found to be composed of 4.7% graupel, 80.8% snow (11.6% dendrite, 0.9% needle/column, and 68.3% undetermined), and 14.5% mixed graupel/snow. Application of the algorithm to the NASA DC-8 2D-CIP data for particles with maximum dimensions greater than $125 \mu\text{m}$ resulted in relative fractions of 0% graupel, 98.4%

snow (0.4% dendrite, 0.8% needle/column, and 97.2% undetermined), and 1.6% mixed graupel/snow. Snow ensembles significantly dominate the UND Citation and the NASA DC-8 particle distributions. The NASA DC-8 graupel and mixed graupel/snow fractions are much smaller than their UND Citation counterparts. The following subsections expand on the characteristics that support the ice particle-type discrimination results.

a. Ice particle-type discrimination as a function of precipitation structure

As discussed in section 3, the aircraft data in this study were examined in the context of precipitation structures derived from the spatial radar reflectivity patterns of an S-band Doppler radar located on Kwajalein Island. Examination of the joint relationship between identified ice particle type of an ensemble and coincident precipitation echo structure provides evidence that supports the veracity of the ice particle-type discrimination algorithm (Table 5). Graupel is usually observed in connection with convective precipitation, while snow particles are more likely to be observed in stratiform precipitation (Houze 1997). Results from the UND Citation indicate that about 64% of the graupel ensembles identified in precipitating echo occurred with

TABLE 5. Number of graupel (GR), snow (SN), and mixed graupel/snow (MGS) particle ensembles from the UND Citation 2DC and NASA DC-8 2D-CIP as a function of their coincidence with convective (CONV) and stratiform (STRAT) precipitation echoes.

	UND Citation			NASA DC-8		
	GR	SN	MGS	GR	SN	MGS
CONV	196	921	370	0	684	9
STRAT	112	3349	376	0	3373	43

convection. Almost all of the stratiform graupel ensembles were within a 10-km horizontal distance of a convective echo. Graupel was identified within or in very close proximity to precipitation structures where its presence would be expected. The spatial distribution of snow was also reasonably consistent with expectations; about 78% of the snow ensembles occurred with stratiform precipitation. About 22% of the snow ensembles occurred in convective echo, which is contrary to theory in a strict sense. This may be partially explained by the common occurrence of embedded convection within stratiform precipitation regions near Kwajalein (Holder et al. 2008). Preexisting snow particles or snow advected from adjacent stratiform regions can coexist with convective precipitation structures especially if the convection is relatively shallow and the microphysical observations are made at higher levels. The convective/stratiform algorithm has a tuning parameter that allows adjustment of convective cell radii to yield smaller convective areas or larger convective areas (Yuter et al. 2005). When these parameters are varied, as in Yuter et al. (2005), 80% of the identified graupel ensembles occur within the larger convective areas. Finally, mixed graupel/snow ensembles from the UND Citation occurred in approximately equal proportions within convective and stratiform precipitation. Given that this category primarily represents snow particles transitioning to graupel, it is plausible that these particles could be found in either convective precipitation or stratiform precipitation near embedded convective cells. For the NASA DC-8, no graupel-dominated ensembles were identified in the entire dataset. The dearth of graupel in the NASA DC-8 dataset is most likely due to these higher fall speed particles either not reaching the NASA DC-8's altitude or having a short residence time at those altitudes. Almost all of the ensembles were identified as snow. Although some mixed graupel/snow ensembles were identified in the NASA DC-8 data, there are too few to draw any conclusions with respect to their coincidence with convective or stratiform precipitation.

b. Temperature distribution as a function of ice particle type

Most of the graupel identified in the UND Citation dataset were sampled at temperatures between 0° and −8°C, although some graupel ensembles were observed at temperatures as cold as −20°C (Fig. 5a). Stith et al. (2004) used a Cloud Particle Imager to identify the habit of individual crystals and found a similar temperature distribution for graupel in the KWAJEX data. These graupel particles were likely uplifted to these levels. Stith et al. (2002) found only traces of supercooled liquid water at −17.5°C during KWAJEX, implying there was not enough supercooled liquid water present at these levels for significant riming growth.

The temperature distribution for UND Citation snow ensembles is much wider than the graupel distribution, with values spanning from −45° to 0°C (Fig. 5b). This broad temperature distribution reflects the different particle shapes (i.e., dendrites, needle/column, and undetermined ensembles) included in the snow category. The majority of the sampled particle ensembles were obtained within multicellular reflectivity regions, which are composed of individual cells in various stages of evolution. Thus a particular ensemble sample volume in these clouds will contain a mixture of particles both formed locally, if the conditions are amenable, and particles formed distant in time and space from the sample volume. For example, stratiform regions, with their generally lower vertical velocities, are typically regions of formerly active convection (Houze 1997), and many ice particles observed in stratiform regions were initially formed in convective regions.

While we cannot definitively identify regions where ice particles have formed, many local maxima in the temperature distributions of the snow subcategories are consistent with temperature regimes in which certain ice crystal types would be expected to grow into recognizable habit forms. For instance, the snow-dendrite temperature distribution ranges from approximately −25° to 0°C with a maximum frequency between −6° and 0°C and a secondary maximum between −11° and −16°C (Fig. 5d). The latter temperature range, from −11° to −16°C, corresponds closely to the preferential growth temperature of dendrites, which can become entangled upon collision more readily than nondendritic crystals (Houze 1993). The local maxima at the temperature range from −6° to 0°C is consistent with sedimentation of dendritic particles formed at higher altitudes (Houze and Churchill 1987). Undetermined snow particles compose ~70% of the snow category; their temperature distribution is essentially the same as the overall snow temperature distribution (Fig. 5e). The breadth of this

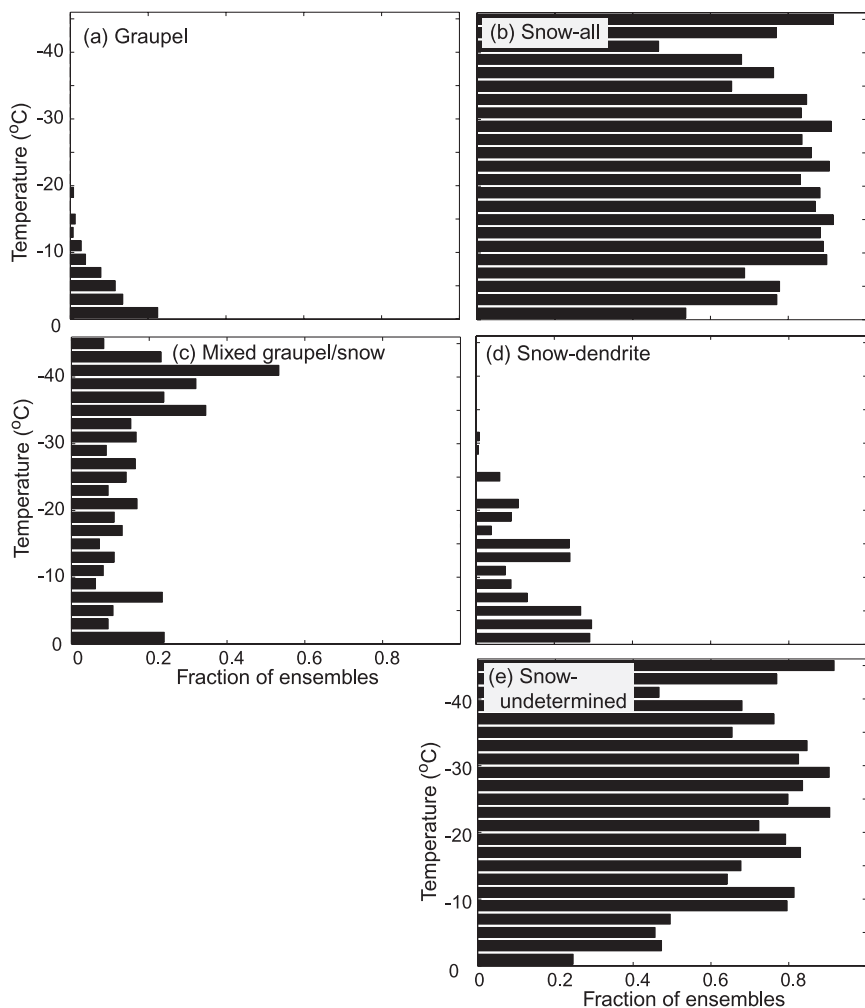


FIG. 5. Temperature distributions of (a) graupel, (b) snow-all (dendrite, needle/column, and undetermined), (c) mixed graupel/snow, (d) snow-dendrite, and (e) snow-undetermined particle ensembles containing at least 100 accepted particles and having temperatures less than 0°C. Distributions are normalized with respect to the total number of ensembles in each temperature bin. Note: snow-needle/column ensembles are not included individually because of their small sample size.

distribution implies that undetermined snow particles might be composed of a wide range of individual crystal types formed in other regions. For example, they could include dendrites and needle/columns whose shape characteristics are masked by the complex configuration of single crystals in the aggregate. Alternatively, they may be composed of polycrystals (Bailey and Hallett 2004).

The UND Citation mixed graupel/snow ensembles (Fig. 5c) have a temperature distribution that reflects both graupel and snow characteristics and encompasses the entire observed temperature range. The NASA DC-8 also had a broad snow temperature distribution with values ranging from approximately -34° to -65°C .

Since the snow category composes greater than 98% of the NASA DC-8 particle images, the temperature distribution is essentially the same as the overall temperature distribution presented in section 3 (Fig. 1b).

c. Particle size as a function of ice particle type

Mean size spectra were constructed for UND Citation graupel, snow, and mixed graupel/snow ensembles (Fig. 6) based on the subset of particles within an ensemble that had maximum dimensions greater than $150\ \mu\text{m}$. Data from the 2DC and the HVPS were combined to obtain these spectra using $50\text{-}\mu\text{m}$ -wide bins centered at $175\text{--}975\ \mu\text{m}$ for the 2DC and $400\text{-}\mu\text{m}$ -wide bins centered at $1200\text{--}24\ 800\ \mu\text{m}$ for the HVPS. A slight

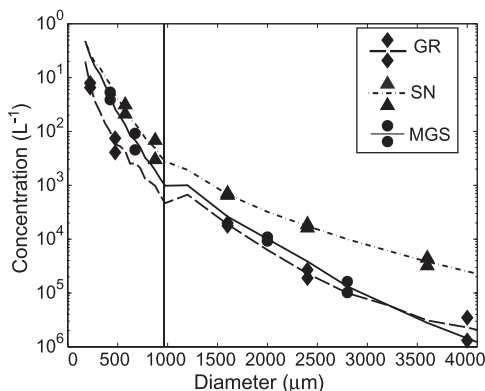


FIG. 6. Mean size spectra for graupel (GR), snow (SN), and mixed graupel/snow (MGS) particle ensembles identified in the UND Citation dataset with their respective positive and negative Poisson distribution values. The vertical line indicates the cutoff between data from the 2DC probe and data from the HVPS probe ($\sim 1000 \mu\text{m}$).

discontinuity in the spectra of the two instruments is evident near $1000 \mu\text{m}$ where the data were merged. In this plot, concentrations for sizes greater than $4000 \mu\text{m}$ are not displayed since the number of particles sampled at those sizes was relatively small, thus reducing the statistical significance of the derived concentrations. Shattering potentially affects the concentration of smaller-sized particles (Korolev and Isaac 2005). Although many of the shattering events are captured and eliminated in the image processing step (see section 4d), we cannot rule out that some portion of the smaller particles in the accepted ensembles is the result of ice particle shattering.

Comparison of the three UND Citation spectra shows that the snow spectrum has larger concentrations than both the graupel and mixed graupel/snow spectra for all sizes greater than $200 \mu\text{m}$. Below $\sim 500 \mu\text{m}$ the mixed graupel/snow spectrum appears to have similar concentrations to the snow spectrum. However, between 600 and $1000 \mu\text{m}$ this similarity ends as the mixed graupel/snow spectrum shifts toward a more graupel-like spectrum. Indeed, between 1200 and $4000 \mu\text{m}$, the mixed graupel/snow and the graupel spectra are very much alike.

Similar to the UND Citation spectra, the NASA DC-8 mean spectra of snow ensembles had larger concentrations than the mixed graupel/snow ensembles (not shown). The mixed graupel/snow spectra were very dissimilar from the snow spectrum, which may be a statistical artifact since there was only a small percentage of ensembles ($\sim 2\%$) identified as mixed graupel/snow in the NASA DC-8 data.

Particle size was further analyzed through examination of the mean volume diameter (the fourth moment of the particle size distribution divided by the third

moment) from the UND Citation graupel, snow, and mixed graupel/snow ensembles. The mean volume diameters for graupel range from 150 to $2000 \mu\text{m}$ (Fig. 7a), with average and median values of 901 and $811 \mu\text{m}$, respectively. In contrast, snow mean volume diameters extend over a broader range, varying from $200 \mu\text{m}$ to $>5 \text{ mm}$ (Fig. 7b), with average and median values of 1280 and $915 \mu\text{m}$, respectively. The larger sizes can be explained by the presence of dendritic snow particles (Fig. 7d). The lower median value relative to the mean is the result of the smaller needle/column ensembles (not shown) and the large number of undetermined snow ensembles that are skewed to smaller sizes than the dendritic ensembles (Fig. 7e).

Similar to graupel, mean volume diameter for the mixed graupel/snow ensembles ranges from 200 to $\sim 2000 \mu\text{m}$ (Fig. 7c). Calculated mean and median values of the mean volume diameter distribution were found to be 772 and $675 \mu\text{m}$, respectively. It is probable that these mean and median values are lower than the graupel values because the mixed graupel/snow category encompasses smaller graupel-like particles.

The mean volume diameter distribution of the NASA DC-8 snow ensembles ranged from 200 to $\sim 1200 \mu\text{m}$ (not shown). This smaller range of sizes most likely reflects the higher altitudes and lower temperatures at which the data were collected and implies that the larger, heavier particles were probably not lofted to these levels from the lower altitudes sampled by the UND Citation. Similar to the UND Citation mixed graupel/snow, the average of the mean volume diameter distribution for the NASA DC-8 mixed graupel/snow was smaller than for the snow particles.

d. Tiny particles

As stated in section 3, $\sim 56\%$ of the individual particle images collected by the UND Citation 2DC and $\sim 65\%$ of particle images collected by the NASA DC-8 2D-CIP were classified as tiny. Although these particles were eliminated from the ice particle-type discrimination analysis because they were too small for accurate ice particle-type identification, the existence of tiny particles can provide a context that helps to explain microphysical processes that may be occurring.

Despite the large number of images classified as tiny, only 3.5% of the ensembles were dominated by tiny particles (i.e., ensembles containing more than 100 tiny particles and having less than 100 accepted particles). In general, most tiny images are embedded in particle ensembles that contain particles with sizes greater than $150 \mu\text{m}$.

Tiny particles may arise for multiple reasons. Instrument malfunction, such as the sporadic image noise that

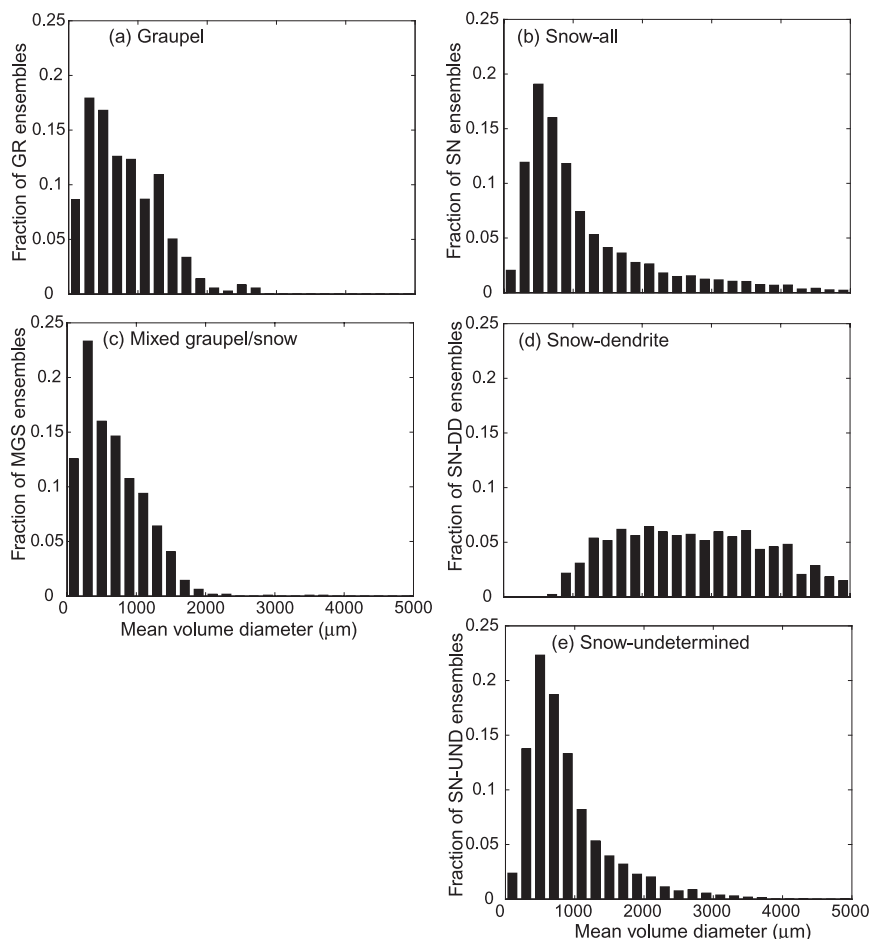


FIG. 7. Mean volume diameter distributions of (a) graupel (GR), (b) all snow (SN; dendrite, needle/column, and undetermined types), (c) mixed graupel/snow (MGS), (d) snow-dendrite (SN-DD), and (e) snow-undetermined (SN-UND) particle ensembles containing at least 100 accepted particles and having temperatures less than 0°C . Distributions are normalized with respect to the total number of ensembles classified in each ice particle type. Note: snow-needle/column ensembles are not included individually because of their small sample size.

sometimes plagues probe electronics, produces tiny particle images. This phenomenon did not appear to occur often in this study, as most tiny images were observed to coexist in ensembles with larger accepted particles, implying that the instrument was working properly. Ice particle shattering also results in tiny particle images (Korolev and Isaac 2005). In this case, when a larger snow particle impacts and shatters on the sides of the probe, a cluster of smaller particles is dispersed into space and these images tend to show up in the data imagery either within the same frame or in multiple frames at successive time intervals. Korolev and Isaac (2005) found that shattered ice images in successive time frames tend to have shorter interarrival times than the average interarrival time. Field et al. (2006) suggest

employing an interarrival time threshold from 1×10^{-5} to 2×10^{-4} s as a means of filtering out shattered images. However, Korolev and Isaac (2005) provided evidence that indicates interarrival time alone cannot be used for identification of shattering events. In this analysis, the image processing step eliminates tiny images found in the same frame (gapped images) and tiny images with zero interarrival time as image artifacts. However, an unknown subset of shattered tiny images will remain in the data and these shattered events cannot be accurately identified. The portion of tiny images that are not the result of shattering is either small ice particles or small supercooled drops. Tiny particles were often observed to coexist with mixed graupel/snow particles and would contribute to riming if the tiny particles were liquid.

5. Summary and conclusions

The variability of graupel and snow in precipitating deep convective clouds over the tropical western Pacific Ocean has been described. Data for this analysis were collected during the KWAJEX field campaign. The principal datasets were obtained by the UND Citation and NASA DC-8 aircraft, both instrumented with 2D-OAPs.

Ice particle types were identified by extending the ensemble-based classification scheme of KS00. Selection of thresholds used in this study was based upon visual analysis of the particle ensembles. The discrimination algorithm that resulted from this comparison (Fig. 2) provides a quantitative method to specifically identify ensembles dominated by graupel and snow particles. A third category, mixed graupel/snow, has characteristics between those of the predominately graupel and snow ensembles and can be used either in combination with the other two categories or separately. For the validation of graupel occurrence in numerical model output, inclusion of mixed graupel/snow with graupel would yield an upper limit to the presence of graupel, while the graupel category by itself would yield a lower limit. A good numerical model would produce a graupel result between those two bounds.

Application of the algorithm to data from the UND Citation and NASA DC-8 was constrained to ensembles at temperatures below 0°C that contained at least 100 accepted particles. Snow ensembles overwhelmingly dominate for both aircraft composing 80% of all ensembles for UND Citation 2DC data and 98% for the NASA DC-8 2D-CIP data. For the UND Citation data, graupel ensembles compose ~5% of the total, with mixed graupel/snow ensembles composing ~15%. This would lead to a lower graupel limit of 5% and an upper graupel limit of 20%, which contradicts numerical model simulation results for this region that imply graupel is dominant in these types of storms (Li et al. 2008). In contrast, no graupel is observed in the NASA DC-8 dataset, and only ~2% of the ensembles were identified as mixed graupel/snow. Tiny particles, which are too small for identification of ice particle type, compose 56% of the UND Citation particle images and 65% of NASA DC-8 particle images and nearly all occur in combination with larger particles.

To provide greater context, the ice particle-type discrimination results were examined relative to radar-derived precipitation structure, air temperature, and particle size spectra. Almost all graupel was either coincident with or within a 10-km horizontal distance of convective precipitation echoes (Table 5). For the UND Citation, more than three-quarters of snow ensembles were observed within stratiform precipitation,

and mixed graupel/snow ensembles were evenly distributed between convective and stratiform precipitation echoes.

Two subcategories, snow-dendrite and snow-needle/column, were identified within the general snow category with the rest of the snow particles falling into the residual snow-undetermined category. For the UND Citation, 68% of snow particles fall into the snow-undetermined subcategory as compared with 97% for NASA DC-8. Given the limitations of the 2D-OAP instruments, we are unable to make an ice particle classification more detailed than “snow” for the vast majority of ice particles sampled during KWAJEX.

Snow and mixed graupel/snow ensembles were evident over the entire range of subfreezing temperatures (from 0° to -45°C) sampled by the UND Citation (Fig. 5). In concurrence with Stith et al.’s (2004) findings for individual particles, graupel ensembles were most prevalent at temperatures greater than -10°C. Graupel occurrence decreased with decreasing temperature until no graupel ensembles were observed at temperatures colder than -20°C. Ensembles identified as snow were characterized by larger number concentrations than those identified as graupel, a difference that increased as particle size increased (Fig. 6). The size spectra of ensembles identified as mixed graupel/snow were similar to snow particles at sizes <500 μm and similar to graupel at sizes >1200 μm.

Acknowledgments. The authors thank all of the scientists and aircraft flight crews who participated in the data collection effort during the TRMM KWAJEX field campaign. We also thank Alexei Korolev, Sergey Matrosov, Roger Reinking, and three anonymous reviewers for providing feedback and helpful suggestions. The work reported in this paper was supported by NASA Grants NAG5-9716 and NNG04GJ15G (Sukovich and Kingsmill) and NASA Grant NNG04GA65G and NSF ATM-0544766 (Yuter).

APPENDIX

Minimum Particle Number Threshold

To obtain reasonable particle ensemble statistics of the ice particle classification algorithm, the fractions of graupel, snow, and mixed graupel/snow in the KWAJEX dataset were calculated using different thresholds for the minimum number of accepted particles in an ensemble (Table A1). At minimum particle thresholds less than or equal to 100, the distribution of UND Citation ice particle types was fairly consistent at 4%–6%

TABLE A1. Calculated percentages and counts (in parentheses) of graupel (GR), snow (SN), and mixed graupel/snow (MGS) ensembles for the UND Citation 2DC and the NASA DC-8 2D-CIP data during TRMM KWAJEX for different minimum particle thresholds.

Min No. of particles	UND Citation			NASA DC-8		
	GR	SN	MGS	GR	SN	MGS
1	5.5% (497)	82.6% (7222)	11.9% (1342)	~0.0% (11)	96.6% (10 838)	3.3% (376)
50	5.1% (411)	80.1% (6431)	14.8% (1186)	0.0% (0)	97.7% (8397)	2.3% (196)
100	4.7% (357)	80.8% (6162)	14.5% (1106)	0.0% (0)	98.4% (7752)	1.7% (130)
500	0.1% (5)	90.6% (3927)	9.3% (402)	0.0% (0)	99.2% (5168)	0.8% (40)

graupel, 80%–84% snow, and 12%–15% mixed graupel/snow. However, for thresholds larger than 100 particles, the mixed graupel/snow fraction decreased substantially, while the graupel fraction decreased to almost zero and the snow fraction increased to about 90%. Similarly, the NASA DC-8 data showed a larger decrease in mixed graupel/snow above the 100 particle threshold. Thus, a 100 particle minimum was required of all accepted particle ensembles in both the UND Citation and NASA DC-8 data that were included in the ice particle-type discrimination analysis. This minimum particle number threshold is supported by other habit identification work (Korolev et al. 2000), which also found that a 100-particle threshold was necessary to maintain statistical significance.

REFERENCES

- Bailey, M., and J. Hallett, 2004: Growth rates and habits of ice crystals between -20° and -70° C. *J. Atmos. Sci.*, **61**, 514–544.
- Baumgardner, D., and A. Korolev, 1997: Airspeed corrections for optical array probe sample volumes. *J. Atmos. Oceanic Technol.*, **14**, 1224–1229.
- Brown, P. R., and H. A. Swann, 1997: Evaluation of key microphysical parameters in three-dimensional cloud-model simulations using aircraft and multiparameter radar data. *Quart. J. Roy. Meteor. Soc.*, **123**, 2245–2275.
- Colle, B. A., M. F. Garvert, J. B. Wolfe, C. F. Mass, and C. P. Woods, 2005: The 13–14 December 2001 IMPROVE-2 event. Part III: Simulated microphysical budgets and sensitivity studies. *J. Atmos. Sci.*, **62**, 3535–3558.
- Czys, R. R., and M. S. Peterson, 1992: A roughness-detection technique for objectively classifying drops and graupel in 2D-image records. *J. Atmos. Oceanic Technol.*, **9**, 242–257.
- Duroure, C., 1982: Une nouvelle methode de traitement des images d'hydrometeores donnees par les sondes bidimensionnelles. *J. Rech. Atmos.*, **6**, 71–84.
- , H. R. Larsen, H. Isaka, and P. Personne, 1994: 2D image population analysis. *Atmos. Res.*, **34**, 195–205.
- Field, P. R., A. J. Heymsfield, and A. Bansemer, 2006: Shattering and particle interarrival times measured by optical array probes in ice clouds. *J. Atmos. Oceanic Technol.*, **23**, 1357–1371.
- Glickman, T., Ed., 2000: *Glossary of Meteorology*. 2nd ed. Amer. Meteor. Soc., 855 pp.
- Gordon, G. L., and J. D. Marwitz, 1984: An airborne comparison of three PMS probes. *J. Atmos. Oceanic Technol.*, **1**, 22–27.
- Heymsfield, A. J., and J. L. Parrish, 1978: A computational technique for increasing the effective sampling volume of the PMS two-dimensional particle size spectrometer. *J. Appl. Meteor.*, **17**, 1566–1572.
- Holder, C., S. E. Yuter, A. Sobel, and A. Ayyer, 2008: The mesoscale characteristics of tropical oceanic precipitation during Kelvin and mixed Rossby-gravity wave events. *Mon. Wea. Rev.*, **136**, 3446–3464.
- Holroyd, E. W., 1987: Some techniques and uses of 2D-C habit classification for snow particles. *J. Atmos. Oceanic Technol.*, **4**, 498–511.
- Houze, R. A., Jr., 1993: *Cloud Dynamics*. Academic Press, 573 pp.
- , 1997: Stratiform precipitation in regions of convection: A meteorological paradox? *Bull. Amer. Meteor. Soc.*, **78**, 2179–2196.
- , and D. D. Churchill, 1987: Mesoscale organization and cloud microphysics in a Bay of Bengal depression. *J. Atmos. Sci.*, **44**, 1845–1868.
- Hunter, H. E., R. M. Dyer, and M. Glass, 1984: A two-dimensional hydrometeor machine classifier derived from observed data. *J. Atmos. Oceanic Technol.*, **1**, 28–36.
- Iguchi, T., T. Kozu, R. Meneghini, J. Awaka, and K. Okamoto, 2000: Rain-profiling algorithm for the TRMM precipitation radar. *J. Appl. Meteor.*, **39**, 2038–2052.
- Kingsmill, D. E., and Coauthors, 2004: TRMM common microphysics products: A tool for evaluating spaceborne precipitation retrieval algorithms. *J. Appl. Meteor.*, **43**, 1598–1618.
- Knollenberg, R. G., 1970: The optical array: An alternative to scattering or extinction for airborne particle size determination. *J. Appl. Meteor.*, **9**, 86–103.
- Korolev, A. V., and B. Sussman, 2000: A technique for habit classification of cloud particles. *J. Atmos. Oceanic Technol.*, **17**, 1048–1057.
- , and G. A. Isaac, 2005: Shattering during sampling by OAPs and HVPS. Part I: Snow particles. *J. Atmos. Oceanic Technol.*, **22**, 528–542.
- , J. W. Strapp, and G. A. Isaac, 1998: Evaluation of the accuracy of PMS optical array probes. *J. Atmos. Oceanic Technol.*, **15**, 708–720.
- , G. A. Isaac, and J. Hallett, 2000: Ice particle habits in stratiform clouds. *Quart. J. Roy. Meteor. Soc.*, **126**, 2873–2902.
- Kummerow, C., W. Barnes, T. Kozu, J. Shiue, and J. Simpson, 1998: The Tropical Rainfall Measuring Mission (TRMM) sensor package. *J. Atmos. Oceanic Technol.*, **15**, 809–817.

- , and Coauthors, 2000: The status of the Tropical Rainfall Measuring Mission (TRMM) after two years in orbit. *J. Appl. Meteor.*, **39**, 1965–1982.
- , and —, 2001: The evolution of the Goddard Profiling Algorithm (GPROF) for rainfall estimation from passive microwave sensors. *J. Appl. Meteor.*, **40**, 1801–1820.
- Lang, S., W. K. Tao, R. Cifelli, W. Olson, J. Halverson, S. Rutledge, and J. Simpson, 2007: Improving simulations of convective systems from TRMM LBA: Easterly and westerly regimes. *J. Atmos. Sci.*, **64**, 1141–1164.
- Lawson, R. P., R. E. Stewart, J. W. Strapp, and G. A. Isaac, 1993: Airborne measurements of the origin and growth of very large snowflakes. *Geophys. Res. Lett.*, **20**, 53–56.
- Li, Y., E. J. Zipser, S. K. Krueger, and M. A. Zulauf, 2008: Cloud-resolving modeling of deep convection during KWAJEX. Part I: Comparison to TRMM satellite and ground-based radar observations. *Mon. Wea. Rev.*, **136**, 2699–2712.
- Lin, Y. L., R. Farley, and H. D. Orville, 1983: Bulk parameterization of the snow field in a cloud model. *J. Climate Appl. Meteor.*, **22**, 1065–1092.
- Locatelli, J. D., and P. V. Hobbs, 1974: Fall speeds and masses of solid precipitation particles. *J. Geophys. Res.*, **79**, 2185–2197.
- Moss, S. J., and D. W. Johnson, 1994: Aircraft measurements to validate and improve numerical model parameterization of ice to water ratios in clouds. *Atmos. Res.*, **34**, 1–25.
- Reisner, J., R. M. Rasmussen, and R. T. Bruintjes, 1998: Explicit forecasting of supercooled liquid water in winter storms using the MM5 mesoscale model. *Quart. J. Roy. Meteor. Soc.*, **124**, 1071–1107.
- Rutledge, S. A., and P. V. Hobbs, 1983: The mesoscale and microscale structure and organization of clouds and precipitation in midlatitude cyclones. VIII: A model for the “seeder-feeder” process in warm-frontal rainbands. *J. Atmos. Sci.*, **40**, 1185–1206.
- Simpson, J., R. F. Adler, and G. R. North, 1988: A proposed Tropical Rainfall Measuring Mission (TRMM) satellite. *Bull. Amer. Meteor. Soc.*, **69**, 278–295.
- Smith, E. A., A. Mugnai, H. J. Cooper, G. J. Tripoli, and X. Xiang, 1992: Foundations for statistical-physical precipitation retrieval from passive microwave satellite measurements. Part I: Brightness-temperature properties of a time-dependent cloud radiation model. *J. Appl. Meteor.*, **31**, 506–531.
- Stith, J. L., J. E. Dye, A. Bansemmer, A. J. Heymsfield, C. A. Grainger, W. A. Petersen, and R. Cifelli, 2002: Microphysical observations of tropical clouds. *J. Appl. Meteor.*, **41**, 97–117.
- , J. A. Haggerty, A. Heymsfield, and C. A. Grainger, 2004: Microphysical characteristics of tropical updrafts in clean conditions. *J. Appl. Meteor.*, **43**, 779–794.
- Stoelinga, M. T., J. D. Locatelli, and C. P. Woods, 2007: The occurrence of “irregular” ice particles in stratiform clouds. *J. Atmos. Sci.*, **64**, 2740–2750.
- Strapp, J. W., F. Albers, A. Reuter, A. V. Korolev, U. Maixner, E. Rashke, and Z. Vukovic, 2001: Laboratory measurements of the response of a PMS OAP-2DC. *J. Atmos. Oceanic Technol.*, **18**, 1150–1170.
- Tao, W.-K., and Coauthors, 2003: Microphysics, radiation and surface processes in a non-hydrostatic model. *Meteor. Atmos. Phys.*, **82**, 97–137.
- Thompson, G., R. M. Rasmussen, and K. Manning, 2004: Explicit forecasts of winter precipitation using an improved bulk microphysics scheme. Part I: Description and sensitivity analysis. *Mon. Wea. Rev.*, **132**, 519–542.
- Yuter, S. E., R. A. Houze, E. A. Smith, T. T. Wilheit, and E. Zipser, 2005: Physical characterization of tropical oceanic convection observed in KWAJEX. *J. Appl. Meteor.*, **44**, 385–415.